On Tidal Motion in a Stratified Inlet, with Particular Reference to Boundary Conditions

CARL E. PEARSON AND DONALD F. WINTER

University of Washington, Seattle, WA 98195

(Manuscript received 21 March 1983, in final form 4 June 1984)

ABSTRACT

The method of characteristics is used to provide radiation-type boundary conditions appropriate to a portion of a two-layer inlet subject to tidal effects governed by one-dimensional shallow-water theory. Internal waves are considered, with Knight Inlet as an example.

1. Introduction

Tidal motion in stratified inlets is of considerable interest to oceanographers and water quality engineers; papers by Crean (1978), Freeland and Farmer (1980), Hamilton (1974), Jamart and Winter (1980), and Baines (1982) are representative of many investigations describing field observations and various experimental or analytical models. If a numerical approach is used to investigate tidal motion, it may be computationally efficient to analyze only that region R of the inlet which is of primary interest (the part containing a sill, for example). The question then arises concerning the choice of appropriate boundary conditions for the two ends of R, and this matter receives particular attention here. We restrict ourselves to one-dimensional situations in which velocities can be averaged laterally and over each density layer, and in which the pressure can be considered hydrostatic, so that shallow water theory is applicable, as described by Stoker (1957), for example. Although this kind of approximation is often invoked, it may be inadequate in regions of rapid change in depth or width, or in the reproduction of short-wavelength phenomena. Moreover, turbulent mixing is not modeled explicitly. Some of these defects can be corrected by subsequent *ad hoc* analyses, in which the shallow water solution provides the environment; in any event, these and other difficulties are common to many analytical approaches. Our main objective here is the fairly modest one of discussing the choice of boundary conditions for the region of interest and, in order to concentrate on this matter, we simplify the model by neglecting wind stress, interfacial shear stress, bottom friction, interlayer mixing, and flow separation at ridges. Some of these effects can readily be incorporated into the model (although it may not be easy to assign realistic numerical values to the various coefficients which arise); e.g., see Hodgins (1979).

First we consider the seaward end of the region R. A natural approach (frequently used in the literature) is to specify the tidal height variation as a function of time—perhaps in terms of the amplitudes and phases of the first few periodic components. Unfortunately, a height specification has the consequence that any disturbance generated within the region and propagating seaward will be reflected back into the region by this boundary condition, thus artificially complicating the subsequent motion. A second difficulty is that the mathematical problem associated with a prescribed-height boundary condition may not be "well posed." Any measured tidal height variation is a consequence of two effects—an imposed forcing function (the incoming tide) and the response of the local geometry (e.g., reflection) to that forcing function. Situations such as this in which one imposes a boundary condition that includes part of the system response can be very sensitive to small changes in the input condition; in fact the apparent necessity of including high-order harmonics in some estuarine tidal models may be attributable to this effect. A further discussion is given by Pearson and Winter (1977) and Jamart (1980). Finally, it is not always clear how the height variation of each of (say) two layers should be specified, unless one takes the seaward boundary sufficiently far seaward that the thickness of the upper layer may be taken as zero there. A related question concerns the effect of initial conditions (frequently corresponding to zero velocity) on water elevation and velocity variation when the forcing function at the seaward end is essentially periodic. In practice, it is often assumed that computed height variations produced by a given distribution of tidal harmonics can be compared directly with measured heights after one or two tidal cycles. However, in low-friction channels, transients persist for longer periods and remain within the modeled section as a result of reflections from the ends. This effect may be illustrated by considering the simple case of tidal motion in a straight inlet of uniform mean depth D.

Suppose that, at $x = L$, there is imposed a sinusoidal variation in surface height with amplitude $2A\cos(2\pi L/cT)$, where T is the period and $c = (gD)^{1/2}$; the velocity at the landward end is zero. If the motion were periodic, the surface elevation would be given by

$$\eta_s(x, t) = A\left[\sin\frac{2\pi}{T}\left(t - \frac{x}{c}\right) + \sin\frac{2\pi}{T}\left(t + \frac{x}{c}\right)\right].$$

However, if the motion is started from rest with zero velocity, the solution can be expressed as the sum of $\eta_s(x, t)$ and a component $\eta_i(x, t)$ associated with the starting conditions:

$$\eta_i(x, t) = \sum_{n=0}^{\infty} B_n\left[\sin\frac{(2n+1)}{2}\frac{\pi c}{L}\left(t + \frac{x}{c}\right) + \sin\frac{(2n+1)}{2}\frac{\pi c}{L}\left(t - \frac{x}{c}\right)\right],$$

where

$$B_n = \frac{4AL}{\pi cT}(-1)^n \frac{\cos(2\pi L/cT)}{[2L/(cT)]^2 - [(2n+1)/2]^2}.$$

The function $\eta_i(x, t)$ represents the discrepancy between the periodic solution and the initial value solution, and can be regarded as a superposition of harmonics traveling landward and seaward, undergoing reflections at each end. When $cT \gg L$, the main contribution is from the first term so that the amplitude of the "transient" relative to the amplitude of the periodic wave is

$$\frac{|B_0|}{A} \approx \frac{16L}{\pi cT}.$$

Thus, for example, in a channel of 40 km length and 150 m depth, at the end of one cycle of an M_2 tide, approximately 12% of the calculated height variation is associated with the starting conditions. The initial transients clearly persist and the tidal response within the segment is comprised of the primary wave as well as an unwanted contribution from the wave reflected from the seaward end.

What is required is a boundary condition that permits seaward propagating disturbances to pass without hindrance, yet one that imposes, in some way, the desired tidal input. It is necessary to adapt to the present situation the "radiation condition" concept of wave–equation theory in which coupled equations in several unknowns appear; e.g., see Carrier and Pearson (1976) and Wurtele *et al.* (1971). If the seaward boundary can be placed in water of sufficient (and locally uniform) depth locally that linearization is feasible then the method of characteristics can be adapted to provide the desired tools. Two of the characteristic curves at this boundary carry information landward, the other two seaward, and these information packages can be combined so as to provide the desired boundary data. We emphasize that the full nonlinear equations are solved numerically in the sill region of interest, and that disturbances emanating from the sill will generally possess contributions arising from nonlinear effects. Although our fjord geometry is such as to make equation linearization valid in the boundary region, it might be remarked that the only crucial consideration is that the boundary be transparent both to the incoming tide and to any reflected disturbances (linear or nonlinear); these criteria are met by the present treatment.

At the landward end of R, similar considerations apply. Thus the boundary condition must be transparent to disturbances propagating landward, yet must take into account whatever basin volume is contained in the remainder of the inlet. Again, the method of characteristics is appropriate; a simple way in which to model the basin volume is to permit disturbances emanating from R to reflect back into R with a time delay corresponding to a suitable geometrically equivalent uniform closed channel. It should be noted that while the boundary conditions are applied in regions where local linearization is feasible, the full nonlinear equations are used throughout the inlet segment of main interest.

2. Numerical time-stepping

The region R to be considered is that lying between $x = 0$ (the seaward boundary) and $x = L$ (the landward boundary) in Fig. (1). A layer of brackish water overlies a saline layer, each of constant density (the density ratio of the former to the latter is r). At time $t = 0$, the lower layer is at rest and the upper layer has a constant velocity U_0' landward (we take $U_0' < 0$). Also at $t = 0$, the lower layer has depth $H(x)$ and the upper layer has constant depth H_0. Let $H(x) = H_1$, constant, for $x < 0$, and $H(x) = H_2$, constant, for $x > L$; the points $x = 0$ and $x = L$ are taken to lie within these constant depth regions. The situation at $t = 0$ as described above corresponds approximately to the end of the ebb tide. Starting at $t = 0$, the tide is "turned on." At time $t > 0$, denote the increases in height at each of the upper surface and the

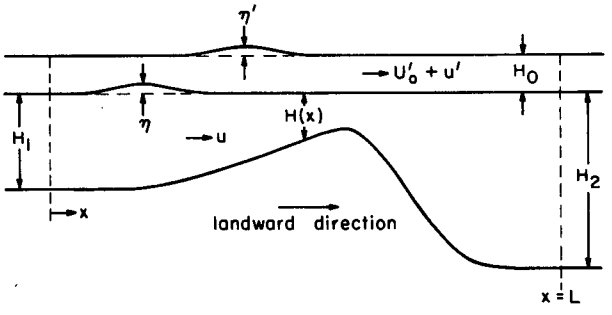

FIG. 1. Geometry of two-layer flow over a sill.

interface by $\eta'(x, t)$ and $\eta(x, t)$ respectively, and denote the corresponding changes in velocities by $u'(x, t)$ and $u(x, t)$, respectively. Thus the instantaneous velocity in the upper layer is $u'(x, t) + U_0'$, taken as positive in the direction of increasing x. We use g to denote the acceleration of gravity, and a subscript to denote a partial derivative. Then the equations of motion are (as by Houghton and Isaacson, 1968; Stoker, 1957)

$$\left.\begin{aligned} u_t &= -\left[\tfrac{1}{2}u^2 + gr\eta' + g(1-r)\eta\right]_x \\ \eta_t &= -[(H+\eta)u]_x, \\ u_t' &= -\left[\tfrac{1}{2}(u')^2 + U_0'u' + g\eta'\right]_x \\ \eta_t' &= -[(\eta' - \eta + H_0)(u' + U_0') + (H+\eta)u]_x \end{aligned}\right\}, \quad (1)$$

or in column vector form,

$$V_t = F_x(V). \quad (2)$$

Various explicit and implicit methods are available for the numerical solution of Eqs. (2) in the region R. We choose here the explicit Lax-Wendroff-Richtmyer method (as described by Richtmyer and Morton, 1957) which has some capability of modeling rapid transitions for conservation-type equations [Eqs. (1) are not in strict momentum- and mass-conservation form. In fact, such a form is awkward to obtain for layered flow (see Houghton and Isaacson, 1968; Yih and Guha, 1955)]; an example of an implicit method is given by Hodgins (1979).

Divide the region $0 < x < L$ into N equal parts, with $\delta x = L/N$; denote the numerical approximation to $V[j(\delta x), n(\delta t)]$ by V_j^n [see Fig. (2)]. Then each δt time step is carried out in two halves. For $j = 0, 1, \cdots (N-1)$, we first compute

$$V_{j+1/2}^{n+1/2} = \frac{1}{2}(V_j^n + V_{j+1}^n) + \frac{(\delta t)}{2(\delta x)}[F(V_{j+1}^n) - F(V_j^n)] \quad (3)$$

so as to provide V values at the intermediate points marked $A_1, A_2 \cdots$ in Fig. (2). The second half step uses

$$V_j^{n+1} = V_j^n + \left(\frac{\delta t}{\delta x}\right)[F(V_{j+1/2}^{n+1/2}) - F(V_{j-1/2}^{n+1/2})] \quad (4)$$

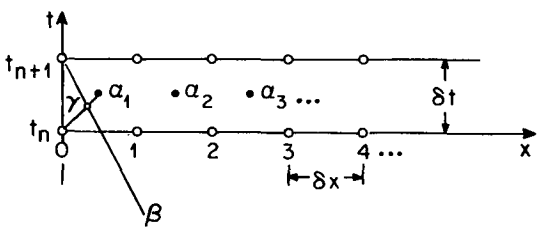

FIG. 2. Computational mesh illustrating the matching of the characteristic solution in the seaward basin with the finite difference solution in the sill segment.

for $j = 1, 2, \ldots, (N-1)$. This process has second-order accuracy and is stable if $\sqrt{gH_{\max}}(\delta t) < (\delta x)$; it does not however provide the end-point values V_0^{n+1} and V_N^{n+1}.

3. Characteristics

As already discussed in Section (1), Eqs. (1) are linearized in the two regions outside R. Thus near $x = 0$ (and also near $x = L$, with H_1 replaced by H_2) we have

$$\left.\begin{aligned} u_t + g(1-r)\eta_x + gr\eta_x' &= 0 \\ \eta_t + H_1 u_x &= 0 \\ u_t' + gr\eta_x' &= 0 \\ \eta_t' + H_1 u_x + H_0 u_x' &= 0 \end{aligned}\right\}, \quad (5)$$

where H_1 is the constant depth of the region $x < 0$. Note that we assume U_0', the surface-layer drift velocity, to be of the same order as the tidal velocities u and u'.

If we try to find solutions of wave form depending only on $(x - ct)$ for some choice of c, then substitution shows that there are four possible values of c, satisfying

$$c^4 - c^2[c_0^2 + (c_0')^2] + (1-r)c_0^2(c_0')^2 = 0, \quad (6)$$

where

$$c_0^2 = gH_1, \quad (c_0')^2 = gH_0. \quad (7)$$

Denote the four roots of Eq. (6) by $\pm c_+$, $\pm c_-$, where $c_+ > c_- > 0$. These are of course the four characteristic slopes. Along each characteristic direction, a particular linear combination of the four dependent variables u, u', η, η' is constant (e.g., see Eq. (4.5) of Houghton and Isaacson, 1968); these are the Riemann invariants. After some algebra, it follows that an equivalent statement is that any solution of Eqs. (5) must have the form

$$\left.\begin{aligned} \eta &= F_+ + F_- + G_+ + G_- \\ u &= \frac{1}{H_1}[c_+(F_+ - G_+) + c_-(F_- - G_-)] \\ r\eta' &= \left(\frac{c_+^2}{c_0^2} + r - 1\right)(F_+ + G_+) \\ &\quad + \left(\frac{c_-^2}{c_0^2} + r - 1\right)(F_- + G_-) \\ u' &= \frac{g}{r}\left(\frac{c_+^2}{c_0^2} + r - 1\right)\left(\frac{F_+}{c_+} - \frac{G_+}{c_+}\right) \\ &\quad + \left(\frac{c_-^2}{c_0^2} + r - 1\right)\left(\frac{F_-}{c_-} - \frac{G_-}{c_-}\right)\Bigg] \end{aligned}\right\}, \quad (8)$$

where F_+, F_-, G_+, G_- are single-variable functions of the form

$$\left.\begin{aligned} F_+ &= F_+(x - c_+t) \\ F_- &= F_-(x - c_-t) \\ G_+ &= G_+(x + c_+t) \\ G_- &= G_-(x + c_-t) \end{aligned}\right\}. \tag{9}$$

The first two of the functions of Eq. (9) represent disturbances traveling to the right, the second two, disturbances traveling to the left.

Eqs. (8) can be rewritten as

$$\left.\begin{aligned} A_1\eta' - A_2\eta + A_3u - A_4u' &= 2(c_+^2 - c_-^2)F_+ \\ A_1\eta' - A_2\eta - A_3u + A_4u' &= 2(c_+^2 - c_-^2)G_+ \\ B_1\eta - B_2\eta' + B_3u' - B_4u &= 2(c_+^2 - c_-^2)F_- \\ B_1\eta - B_2\eta' - B_3u' + B_4u &= 2(c_+^2 - c_-^2)G_- \end{aligned}\right\}, \tag{10}$$

where

$$\left.\begin{aligned} A_1 &= rc_0^2 & B_1 &= c_+^2 + (r-1)c_0^2 \\ A_2 &= c_-^2 + c_0^2(r-1) & B_2 &= rc_0^2 \\ A_3 &= \frac{A_2c_+}{g(r-1)} & B_3 &= \frac{rc_+^2c_-}{g(r-1)} \\ A_4 &= \frac{rc_-^2c_+}{g(r-1)} & B_4 &= \frac{B_1c_-}{g(r-1)} \end{aligned}\right\}. \tag{11}$$

We interpret the functions of Eq. (9) as depicting disturbances which enter a region initially at rest, except for the constant drift velocity U_0' in the upper layer. Thus, still considering the region $x < 0$, the functions F_+ and F_- represent a landward propagating tidal motion, and G_+ and G_- represent seaward propagating disturbances generated by tidal effects in the region $x > 0$.

There is some arbitrariness in depicting the incoming tide; for definiteness and for simplicity, here we set $F_- = 0$ (still for the region $x < 0$), and choose, for example,

$$F_+ = A \sin^2[\pi(x - c_+t)/L_0], \tag{12}$$

where L_0 is the tidal wavelength. (Because of reflection from the inlet head the resultant tidal amplitude will approximate $2A$.) At $t = 0$, the disturbance defined by Eq. (12) is just entering the previously undisturbed region R at the point $x = 0$. Higher harmonics could of course be included. With the choice $F_- = 0$ (and with $G_+ = G_- = 0$ for $t < 0$), Eqs. (8) show that $\eta' \approx \eta$ and $u' \approx u$, insofar as incoming tidal effects are concerned.

For $t > 0$, we now know F_+ [from Eq. (12)] and $F_- = 0$, so that the left-hand sides of the first and third of Eqs. (10) are known at $x = 0$. We do not know G_+ or G_-. However, G_+ is a function of $x + c_+t$, and so must be constant along any line $x + c_+t$ = constant. In the time-step discussion of Section 2, all values of V were obtained except for V_0^{n+1} and V_N^{n+1}. From the mesh point corresponding to $x = 0$, $t = (n + 1)\delta t$ in Fig. (2), draw the line β satisfying the condition $x + c_+t$ = constant, and let it cut the line joining the two points $[x = 0, t = n(\delta t)]$ and $[x = \frac{1}{2}\delta x, t = (n + \frac{1}{2})\delta t]$ at the point B. Since the left-hand side of the second of Eqs. (10) is known at the end points of the latter line, it is obtainable at B by interpolation. The left-hand side of the second of Eqs. (10) must then have this same value at the point $[x = 0, t = (n + 1)\delta t]$. Similarly, we can evaluate the left-hand side of the fourth of Eqs. (10) by use of a line satisfying $x + c_-t$ = constant, so that *in toto* the left-hand sides of each of Eqs. (10)

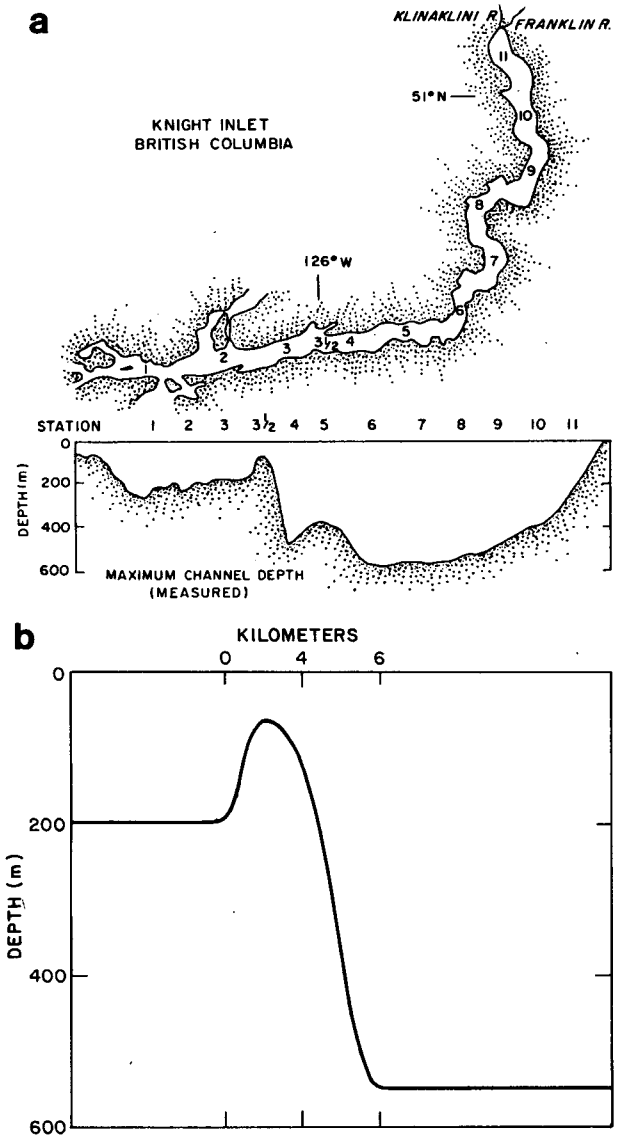

FIG. 3. (a) Knight Inlet, B.C., and the depth profile along the axis of the fjord. (b) Approximate representation of axial depth profile used in the computation.

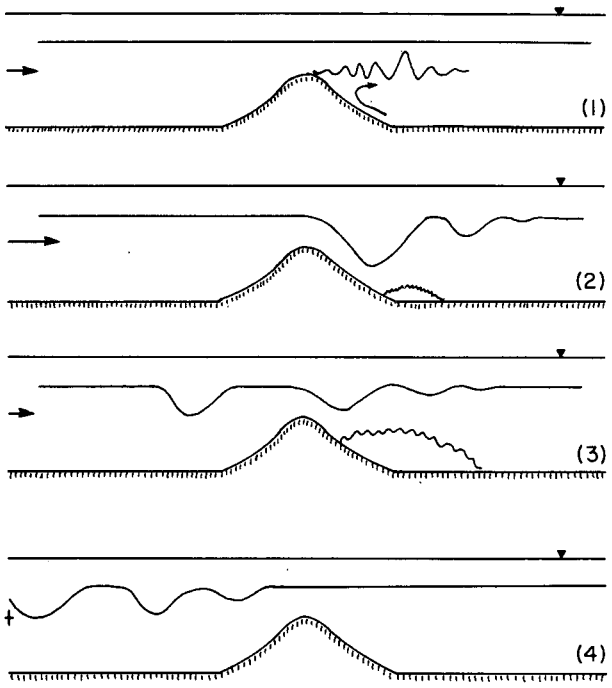

FIG. 4. Schematic diagram illustrating tidally induced flow features in the vicinity of the Knight Inlet sill. The sketch represents a composite of the observed response using density and velocity profilers together with high-frequency echo sounders. The arrows to the left indicate different flow intensities from left to right, starting near the onset of flood tide. The wavy line indicates the possible location of a shear zone in the deep layer. (Reproduced with permission of Plenum Press; see Farmer and Smith, 1980).

are known at the point $x = 0$, $t = (n + 1)\delta t$ and, by solving the linear equation set, V_0^{n+1} can be determined.

At $x = L$, the situation is analogous, except that H_1 must be replaced by the new depth H_2 in the calculation of c_+, c_-, c_0. Disturbances emanating from the region R will propagate towards the head of the inlet, and after reflection, will eventually reenter R. There may be a decay in amplitude, and an added time delay, because of bottom friction. In principle, both of the exiting F_+ and F_- waves could be included in the reflection calculation, but since we intend to model the effect of the basin volume only approximately in any event, we will content ourselves with including the predominant F_+ wave only. (Note that the existence of the F_- wave is a result of the presence of the thin upper layer.) Thus one of the conditions resulting from Eqs. (10), to be applied at $x = L$, is

$$\frac{\partial}{\partial t}[A_1^*\eta' - A_2^*\eta - A_3^*u + A_4^*u']_t = \frac{\partial}{\partial t}[A_1^*\eta' - A_2^*\eta + A_3^*u - A_4^*u']_{t-(2L_b/c_+)}, \quad (13)$$

where subscripts denote evaluation time, L_b is the equivalent basin length and an asterisk denotes a coefficient value involving H_2 rather than H_1. Note that the signs of the u and u' terms differ in the two sides of this equation. Since we neglect the reflection of the F_- wave, a second condition, corresponding to the choice $G_- = 0$, is

$$B_1^*\eta - B_2^*\eta' - B_3^*u' + B_4^*u = 0.$$

The other two conditions are obtained by drawing two lines into the region R, from the point $[x = L, t = (n + 1)(\delta t)]$, with slopes c'_+ and c'_-, and by carrying out interpolation calculations of the kind used at $x = 0$. The resulting four linear equations are solved to give V_N^{n+1} and the time step is now complete.

4. Numerical results

In addition to the usual kinds of numerical checks, several examples of single- and double-layer problems,

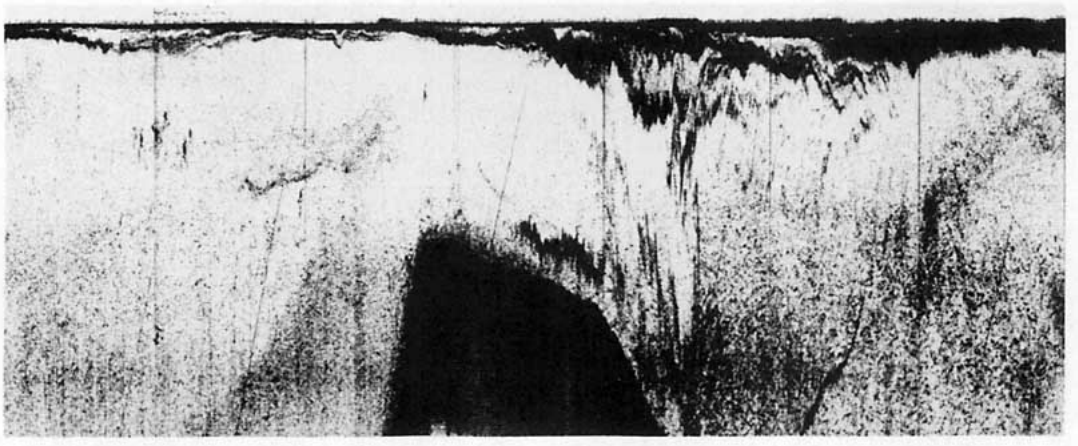

FIG. 5. Portion of an acoustic record showing the development of a lee wave downstream (to the right) of the Knight Inlet sill. (Courtesy of D. M. Farmer.)

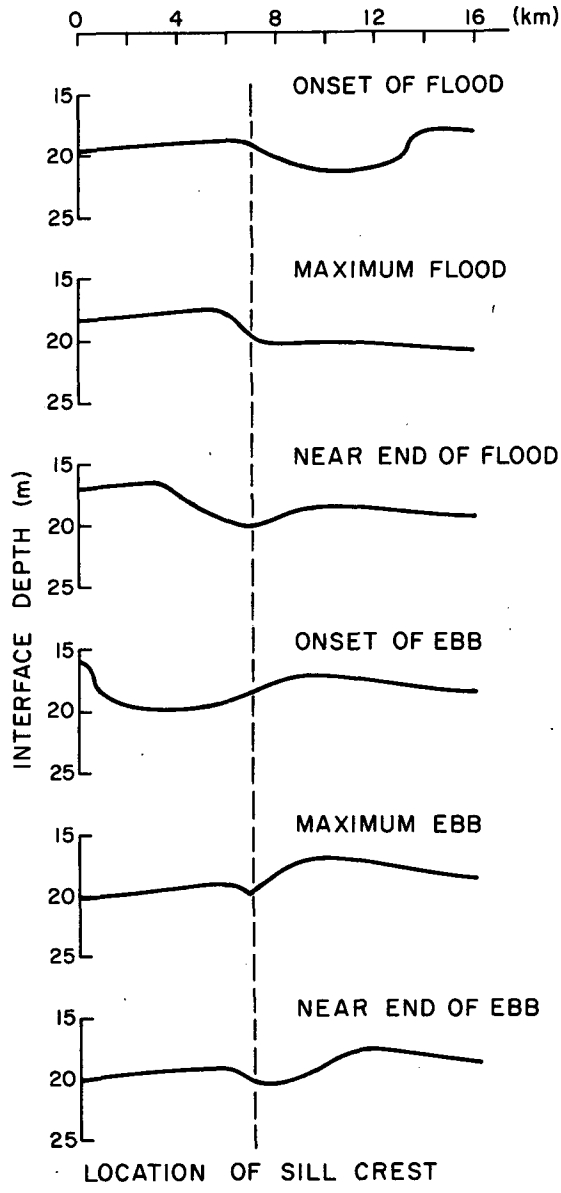

FIG. 6. Computed layer interface configurations at seven different times during the tidal cycle in Knight Inlet.

with known exact solutions, have been solved by the present method. For example, exact solutions are available for the case in which the depth is everywhere constant, and in which the linearized equations are postulated to be exact. The agreement in these cases has been very satisfactory, and no spurious reflections have occurred.

A more interesting problem is that in which an M_2 tide of the type described in Eq. (12) is incident on a region containing a sill. By way of example, the numerical procedure presented here was applied to tidal flow in the vicinity of the inner sill of Knight Inlet. Knight Inlet is a narrow (3 km in width) highly stratified fjord on the British Columbia coastline (see Fig. 3). It is over 100 km long and its bathymetry is characterized by two thresholds, the inner sill being about 8 km long and of approximately 63 m depth at the shallowest point. The sill separates a deep (550 m) inner basin from a shallower (200 m) basin in the seaward reach of the fjord. The bathymetry and the large tidal amplitude (3 to 5 m) produce tidal currents in the vicinity of the inner sill in excess of 80 cm s^{-1}. Moreover, because of seasonally high freshwater runoff into the head of the channel, the surface water in Knight Inlet is often highly stratified. A variety of wave phenomena associated with tidal motion over the inner sill was observed during a series of cruises in the Inlet begun in 1977. Acoustic records and velocity and CTD profiles revealed several tidally induced flow features including internal waves, hydraulic jumps, vortex generation, and boundary separation (see Farmer and Smith, 1980). Figure 4 is a schematic composite of the development and evolution of tidally induced flow features in the vicinity of the Knight Inlet sill and is based upon a large number of acoustic records and CTD profiles acquired in the inlet.

One of the most prominent features seen both in the field experiments and in laboratory simulations is a lee wave which forms on the downstream side of the sill. As the flow diminishes in strength, the wave moves back over the sill and eventually reforms on the other side as the current reverses direction. Figure 5 shows a portion of an acoustic record where the development of a lee wave can be seen as a pronounced thickening of the upper brackish layer, appearing as the dark-colored near-surface zone in the acoustic record.

The numerical procedure described here was used to study the formation and evolution of lee waves in the vicinity of a sill configuration similar to that of Knight Inlet (see Fig. 3b). The total length of the sill was taken to be 8 km. The inner basin on the landward side of the sill was represented as an 80 km channel of 550 m depth, with a wall at the head. The outer basin depth was taken to be 200 m. An M_2 tide with an amplitude of 2 m was imposed at the seaward end of the outer basin. Stratification was simulated by a two-layer flow in which the upper layer was assigned a reference thickness of 20 m and a depth-averaged density of 1022 kg m^{-3}. The density of the deep layer was taken to be 1024 kg m^{-3}. The effect of river discharge was modeled by a persistent seaward current of 2 cm s^{-1} in the upper layer. The computation was started from rest and continued through two tidal cycles to allow transients to propagate out of the system.

Figure 6 shows a sequence of computed layer interface configurations in the segment embracing the sill throughout a tidal cycle. At the onset of flood, the flow over the sill induces a lee wave in the downstream direction. As the current intensifies to-

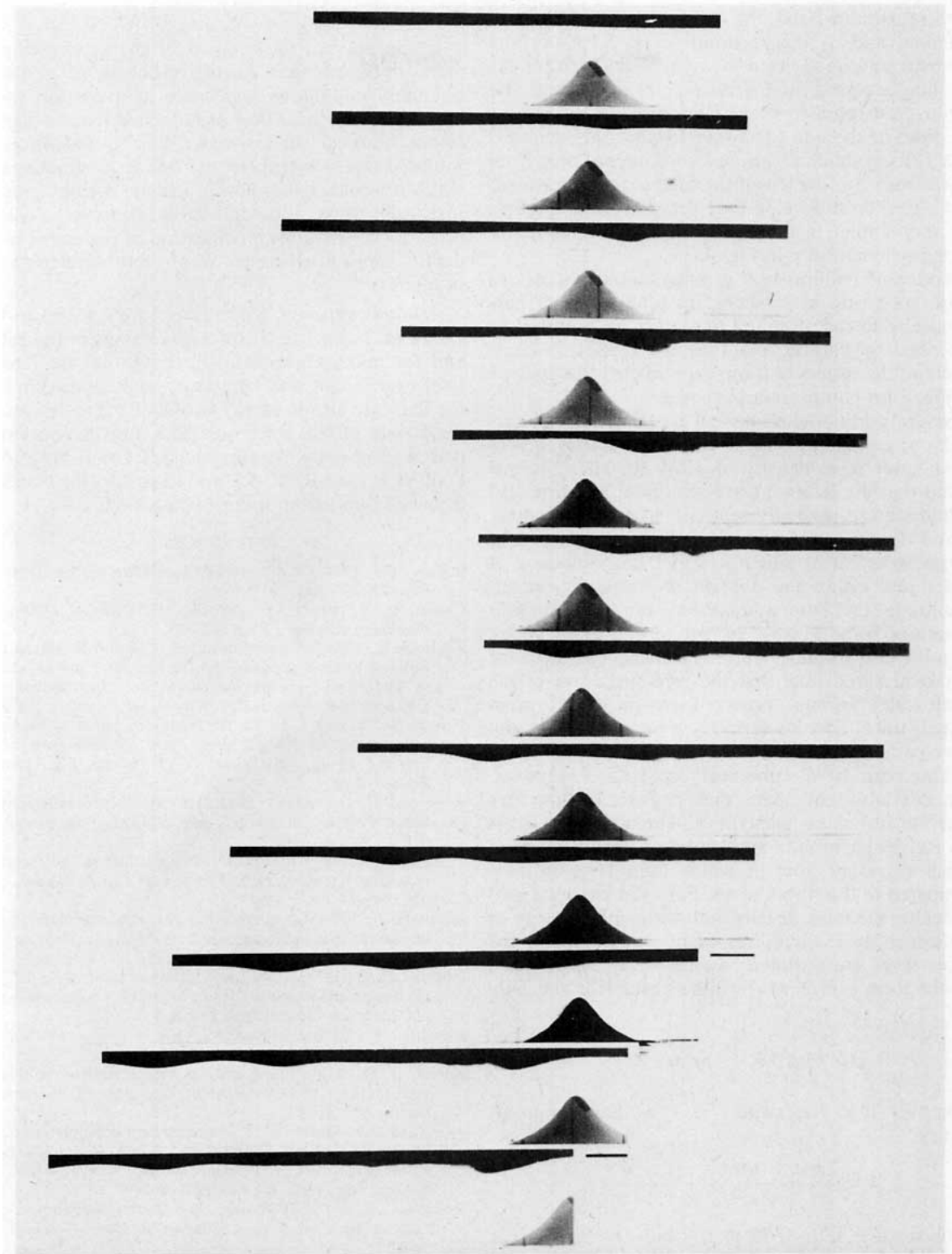

FIG. 7. Sequence of photographs taken at intervals during a laboratory tank study of harmonically forced flow over an obstacle. The obstacle is moved to the left and then to the right relative to the tank and the photographs are positioned so that their frame of reference is fixed with respect to the obstacle. (Laboratory experiment by D. Farmer and J. Zelt. Reproduced with permission of Pergamon Press.)

ward maximum flood, the wave crest broadens considerably and a second minor crest forms in the downstream direction (to the right of the picture). As the flow slackens, the principal lee wave and the minor crest begin to move back over the sill and at the onset of ebb tide a lee wave forms on the seaward side. During ebb flow the crest continues to propagate downstream (to the left of the segment) and a trough and a new crest develop over the sill. These features are very similar to those seen in the field, as represented schematically in Fig. 4.

The same features bear a remarkable similarity to those appearing in a laboratory tank study of harmonically forced stratified flow over an obstacle, as described by Farmer and Freeland (1983). A composite of the results of those experiments is displayed in Fig. 7 for comparison purposes.

Several additional numerical experiments were carried out using the Knight Inlet bathymetry and a fixed lower layer density of 1024 gm cm^{-3}. It was found that the internal wave structure, location, and amplitude are generally sensitive to tidal amplitude A and density ratio r, particularly in the parameter ranges $A \geq 2.0$ m and $r \geq 0.999$. For values of A and r just within the domain of sensitivity, small-amplitude oscillations appeared on the interface waveform, some with wavelength several times greater than the grid spacing. We interpret these as incipient instabilities and note that they are suggestive of the small-scale "billows" observed on the waveform in Knight Inlet. There is certainly a possibility that any wave pattern, particularly if correlated with the mesh spacing, can be a numerical oscillation. However, one can also anticipate that any shear flow can generate turbulent instabilities. The simplest case is the Kelvin-Helmholtz analysis of an inviscid, irrotational two-layer flow in which each layer is deep compared to the wavelengths. For example, let ρ' and u' denote the mass density and horizontal velocity of the upper layer; the corresponding quantities in the lower layer are ρ and u. An interface perturbation for the form $\exp(i2\pi x/\lambda)$ will be unstable if and only if

$$g(\rho^2 - \rho'^2) < \frac{2\pi}{\lambda}\rho\rho'(u - u')^2.$$

Moreover, if $\rho' = r\rho$ (with $r \approx 1$) we have, approximately,

$$\lambda < \frac{2\pi}{g}\frac{(u - u')^2}{1 - r^2} \sim \frac{\pi(u - u')^2}{g(1 - r)}.$$

Thus for $u - u' = 0.50$ m s^{-1} and $r = 0.998$, it is found that $\lambda < 40$ m for instability, which would begin to evidence itself with the mesh spacing used in our computation. Smaller wavelengths, while more unstable, would involve more dissipation. Of course, these results are appropriate to a discontinuous velocity field; more elaborate calculations for shear-gradient flows are available in the literature.

5. Conclusion

It appears that the method of characteristics provides one approach to the problem of choosing boundary conditions applicable to a portion of an inlet subject to tidal flow as governed by one-dimensional stratified shallow-water theory. Extension to multiple layers is feasible, as well as to situations in which it would be desirable to include bottom friction, interfacial stress, and wind stress. However, shallow-water theory requires modification in regions of rapid depth change or where waves of short wavelength are of interest.

Acknowledgments. The authors are grateful to Dr. David M. Farmer for helpful discussions of fjord flow and for making available the results of the Knight Inlet experiment and laboratory tank simulations to us. They are also indebted to one of the reviewers for the Baines (1982) reference. This research was supported in part by Washington Sea Grant NA81AA-D-0030, Project R/NE-12, and in part by the National Science Foundation under MCS-8306592.

REFERENCES

Baines, P. G., 1982: On internal tide generation models. *Deep-Sea Res.*, **29**, 307–338.

Carrier, G. F., and C. E. Pearson, 1976: *Partial Differential Equations.* Academic Press, 320 pp.

Crean, P. B., 1978: A numerical model of barotropic mixed tides between Vancouver Island and the Mainland and its relation to studies of the estuarine circulation. *Hydrodynamics of Estuaries and Fjords,* J. C. J. Nihoul, Ed., Elsevier, 283–313.

Farmer, D. M., and J. D. Smith, 1980: Generation of lee waves over the sill in Knight Inlet. *Fjord Oceanography,* H. J. Freeland, D. M. Farmer and C. D. Levings, Eds., Plenum Press, 715 pp.

——, and H. J. Freeland, 1983: The physical oceanography of fjords. *Progress in Oceanography,* Vol. 12, Pergamon, 147–110.

Freeland, H. J., and D. M. Farmer, 1980: Circulation and energetics of a deep, strongly stratified inlet. *Can J. Fish. Aquatic Sci.*, **37**, 1398–1410.

Hamilton, P., 1974: A numerical model of the vertical circulation of tidal estuaries and its application to the Rotterdam Waterway. *Geophys. J. Roy. Astron. Soc.*, **40**, 1–21.

Hodgins, D. O., 1979: A time-dependent two-layer model of fjord circulation and its application to Alberni Inlet, British Columbia. *Estuarine Coastal Mar. Sci.*, **8**, 362–378.

Houghton, D. D., and E. Isaacson, 1968: Mountain winds. *Stud. in Num. Anal.*, **2**, S.I.A.M., 21–52.

Jamart, B. M., 1980: Finite element computation of barotropic tidal motions, Ph.D. dissertation, University of Washington, Seattle, 148 pp.

——, and D. F. Winter, 1980: Finite element computation of the barotropic tides in Knight Inlet, British Columbia. *Fjord Oceanography,* H. J. Freeland, D. M. Farmer and C. D. Levings, Eds., Plenum Press, 283–289.

Pearson, C. E., and D. F. Winter, 1977: On the calculation of tidal currents in homogeneous estuaries. *J. Phys. Oceanogr.*, **7**, 510–531.

Richtmyer, R. D., and K. W. Morton, 1957: *Difference Methods for Initial Value Problems,* 2nd ed. Wiley, 405 pp.

Stoker, J. J., 1957: *Water Waves.* Interscience, 567 pp.

Wurtele, M. G., J. Paegle and A. Sielecki, 1971: The use of open boundary conditions with the storm-surge equations. *Mon. Wea. Rev.*, **99**, 537–544.

Yih, C. S., and C. R. Guha, 1955: Hydraulic jump in a fluid system of two layers. *Tellus,* **7**, 358–366.